MPHYS PROJECT

Modelling interfacial adsorption of monoclonal antibody COE-3 at the solid/water interface

August 22, 2020

9013483
University of Manchester
School of Physics & Astronomy
Thomas J Leyshon

Abstract

A computational model was produced to simulate COE-3 adsorption at the bare SiO_2/water interface in order to analyse the effects of varying bulk properties; COE-3 concentration, pH and Ionic strength. The model was based on a DLVO theory framework. The simulations were compared to Spectroscopic Ellipsometry (SE) data. Good correlations were observed between the two. The surface tension components of COE-3 were deciphered through the comparisons between the model and experimental data; giving values of γ_3^{lw} = 24.35 mN/m, γ_3^d = 31.05 mN/m and γ_3^a = 18.90 mN/m. The model was then used to provide an understanding of the effects that varying solution environments (COE-3 concentration, pH and ionic strength) have on the underlying dynamics of protein adsorption.

Contents

INTRODUCTION

Understanding the structural deformations and key mechanisms involved in antibody adsorption will provide improved methods for the production and storage of medically used antibodies [1]. Interfacial adsorption at the hydrophilic silicon oxide/water interface is particularly relevant as the silicon oxide surface is a good model of glass, which is widely used to make containers and syringes [2]. Adsorption to the surface of the liquid, the wall of the container and any other material in contact may reduce the desired medical dose. The exact nature of adsorbed COE-3 layers and their impact on the remaining dispersed molecules has had little previous exploration.

Since the development of modern medicine the dynamics of dispersed proteins within aqueous media has been of great scientific interest [3]. From a theoretical point of view the major advances in our understanding of protein interactions has come from the development of DLVO (Derjaguin, Landau, Vervey, and Overbeek) theory in the 1900s [4] [5]. DLVO theory provides a mathematical description of aggregation behaviour between colloidal particles and planar substrates [6]. The theory is based on the energy balance between attractive and repulsive interaction, primarily focusing on attractive van der Waals and repulsive coulombic interactions [7]. Developments of the theory have incorporated the effects of varying environmental bulk properties. These developments are utilised in this model.

COE-3 is of human IgG1k type with a molecular weight of $144,750Da$ and an isoelectric point (pI) of 8.44 . The molecular structure of any monoclonal antibodies (mAbs) consists of one fragment crystallization unit (Fc) and 2 fragment antigen binding units (Fabs) connected in a Y-shape. These 3 components are covered with polar, apolar and charged amino acid groups. The distribution of the amino acid groups causes mAbs to be amphilphilic[1] [8]. Monoclonal antibodies are clones of a single parent cell, they have a wide variety of medical and biotherapeutic applications.

THE MODEL

Interaction forces, Gibbs free energy & surface tensions

According to the second law of thermodynamics, for systems at fixed temperature and pressure a natural tendency for the system to achieve a minimum of the Gibbs free energy exists [9]. Therefore, reactions take place in order to drive the system to a state of equilibrium. At equilibrium the Gibbs potential of the system will be minimized. In this model the Gibbs potential will be used to quantify the evolutionary dynamics of adsorption.

The dynamics are defined by the interactions between the protein, the substrate and the liquid

[1] Possessing both hydrophilic and hydrophobic parts.

medium. These interactions can be understood via DLVO theory, which considers three main contributions: Lifshiftz - Van der Waals (LW), donor/acceptor interactions (DA) and electrostatic forces (EL) [10]. The combined outcome of these individual components dictate the energetics of the adsorption process. Other forces that are involved in extended DLVO theory have been ignored in this model. As these tend to have a much smaller influence then the previous three stated [7].

LW and DA contributions can be expressed in terms of surface tension components via combination laws. While the EL contributions are expressed via surface potentials. Once these individual contributions have been computed separately the resultants can be summed together to form the total Gibbs potential of the interaction, $G(z)_{i2j}$ [10]. The interaction between body i and body j a distance z apart in a liquid medium, 2 is given by

$$G(z)_{i2j} = G(z)^{LW}_{i2j} + G(z)^{DA}_{i2j} + G(z)^{EL}_{i2j}. \tag{1}$$

There are two types of interacting bodies to consider in the adsorption process, these are substrate - protein and protein - protein interactions. Within the DVLO theory framework LW and DA Gibbs potentials can be expressed in terms of the surface tensions of the interacting bodies and medium. This is favourable as the surface tension of a body i, Y_i is an experimentally measurable quantity [11]. Y_i can be split into LW and DA components via

$$Y_i = \gamma^{lw}_i + 2\sqrt{\gamma^d_i \gamma^a_i}. \tag{2}$$

Equation 2 allows for each surface tension component to be determined. Subsequently, the corresponding Gibbs potential of each component and adsorption dynamics can then be determined.

Litshitz - Van der Waals contributions

In equation 1 the LW and DA Gibbs potentials rely on knowing combined values of surface tensions. The Good - Girifalco - Fowkes combination rule for LW interactions between material i and j can be applied [12]. The rule is given by

$$\gamma^{lw}_{ij} = (\sqrt{\gamma^{lw}_i} - \sqrt{\gamma^{lw}_j})^2 \tag{3}$$

with this expression for γ^{lw}_{ij}, the interaction energy between bodies 1 (silica) and 3 (COE-3) in a liquid medium 2 can be expressed using the Dupré equation[2] given below

$$G^{LW}_{123} = \gamma^{lw}_{12} - \gamma^{lw}_{13} - \gamma^{lw}_{23} \tag{4}$$

and for the interaction energy between two bodies of type 3 (COE-3) in a liquid medium 2 the Dupré equation reduces to

[2]The Dupré equation relates the Gibbs potential of the interaction to the interfacial energies of the interaction [10].

$$G_{323}^{LW} = -2\gamma_{23}^{lw}. \tag{5}$$

Equations 3 and 4 describe the Gibbs potential contribution of the LW force between two planes a distance of $l_0 = 0.157nm$ apart [10]. These components do not yet have a z dependence. For the set up of a uniform hard sphere (protein) interacting with a semi-infinite planar surface (silica substrate), the z dependent LW Gibbs potential is given by

$$G(z)_{i2j}^{LW} = \frac{2\pi l_0^2 R G_{323}^{LW}}{z} \tag{6}$$

where z is the distance between the body i and j, R denotes the radius of the hard sphere.

Donor acceptor contributions

The combination rule for DA interactions is given by

$$\gamma_{ij}^{da} = 2(\sqrt{\gamma_i^d} - \sqrt{\gamma_j^d})(\sqrt{\gamma_i^a} - \sqrt{\gamma_j^a}) \tag{7}$$

the DA interaction energy between silica, 1 and COE-3, 3 in a liquid 2 is given by the DA Dupré equation

$$G_{123}^{DA} = \gamma_{12}^{da} - \gamma_{13}^{da} - \gamma_{23}^{da} \tag{8}$$

and for the DA Gibbs potential of interaction between COE-3 and COE-3 this reduces to

$$G_{323}^{DA} = -2\gamma_{23}^{da}. \tag{9}$$

Again, these describe the Gibbs potential contribution of the DA force between two planar surfaces a distance of $l_0 = 0.157nm$ apart [10]. Taking into account the distance z between a hard sphere and a semi-infinite plane, the form of the z dependent DA Gibbs potential is given by

$$G_{i2j}^{DA} = 2\pi\chi R G_{i2j}^{DA} e^{1/\chi(l_0 - z)} \tag{10}$$

where χ is the decay length of the DA interaction with a value taken as $1nm$ [10].

Electrostatic contributions

Unlike the LW and DA Gibbs potential contributions the EL contributions do not depend on surface tensions. But, instead depends upon the surface potentials of the interacting bodies, denoted ψ_i and ψ_j, the EL Gibbs potential is given by

$$G(z)_{i2j}^{EL} = 4\pi R\epsilon_0\epsilon_r\psi_i\psi_j ln[1 + \exp(-\kappa z)] \tag{11}$$

where ϵ_0 and ϵ_r are the vacuum and relative permittivity of the medium respectively ($\epsilon_{r_{water}} = 77.6$ [13]), and

$$\kappa = (\frac{2000e^2 N_A I}{\epsilon_0 \epsilon_r k_B T})^{\frac{1}{2}} \tag{12}$$

where $\frac{1}{\kappa}$ is known as the Debye screening length, e represents the electron charge, k_b is Boltzmann's constant, N_A is Avogadro's number, T and I denotes the solution temperature (Kelvin) and ionic strength (Molar) respectively. The Debye screening length has units of m^{-1} and represents the rate at which charge is screened by the medium [12]. To determine the EL contributions both the surface potentials of silica, ψ_1 and COE-3, ψ_3 need to be deciphered.

Surface potential of silica

Silica is an amphoteric[3] surface. By knowing silica's isoelectric point, pH_0 and ionisation constant, ΔpK silica's surface potential can be calculated via

$$\frac{1}{\alpha}\sinh\left(\frac{y}{2}\right) = \frac{\sigma sinh(2.303\Delta pH - y}{1 + \sigma cosh(2.303\Delta pH - y)} \tag{13}$$

in which y is the dimensionless potential given by $y = \frac{\Psi e}{k_b T}$, $\Delta pH = pH_0 - pH$ with pH being that of the liquid medium. $\sigma = 2x10^{-\Delta pK/2}$ and $\alpha = \frac{N_s \kappa}{4N_A I}$. N_s represents the number of binding sites on the silica surface per a unit area and is commonly taken to be $8nm^{-1}$ [2]. When an amphoteric surface is immersed in a liquid the immediate surrounding solution pH is altered by the potential via

$$pH_{surrounding} = pH + \frac{y}{2.303} \tag{14}$$

this is then the pH that the adsorbed COE-3 layer are occupied within [14].

Surface potential of COE-3

It is common practice to approximate that the antibody surface potential, ψ_3 is equal to its zeta potential, ζ. Where zeta is a potential associated with the collective charge of both the protein and any solution ions within the slipping plane[4] [15]. As the zeta potential incorporates ions from the medium it will not be exactly equal to the surface potential of the protein. However, in reality solution ions do bind to the protein which will change the surface charge and potential. So, incorporation of the slipping plane ions incorporates this ion binding effect [16].

By approximating that the solution is a monovalent[5] medium, the zeta potential and the collective charge is given by

[3] Possessing the ability to react both as a base and as an acid, a characteristic usually found in metal oxides.

[4] The plane enclosing the stationary layer of fluid attached to the dispersed protein [15].

[5] An atom, ion, or chemical group with a valence of one, which thus can form one covalent bond. Note that the medium was actually polyvalent.

$$Q = 2\frac{eR^2\kappa}{l_B} sinh(\frac{\zeta}{2})[1 + \frac{2}{(\kappa R)cosh^2(\frac{\zeta}{2})} + \frac{8log(cosh^2(\frac{\zeta}{4}))}{(\kappa R)^2 sinh(\frac{\zeta}{2})}]^{0.5} \quad (15)$$

where the dimensionless zeta potential is given by $\tilde{\zeta} = \frac{\zeta e}{k_B T}$, and $l_B = \frac{e^2}{4\pi\epsilon_0\epsilon_r k_b T}$ is known as the Bjerrum length [17].

Combining the contributions, Gibbs distribution and implementation

Combining the Gibbs potential contributions of LW, DA and EL results in the overall Gibbs distribution. This was done for both silica - COE-3 and the COE-3 - COE-3 interactions. From these distributions all properties and dynamics of the adsorption process can be determined. Figure 1 shows examples of the Gibbs distributions for both these interaction types, notice in part a) that there are two minimums. The first minimum is not possible for proteins to occupy due to the Born repulsion limit [10]. The second minimum is what drives adsorption. Dispersed molecules feel an attractive force to this minimum energy point. Part b) shows the mutual repulsion between the protein molecules.

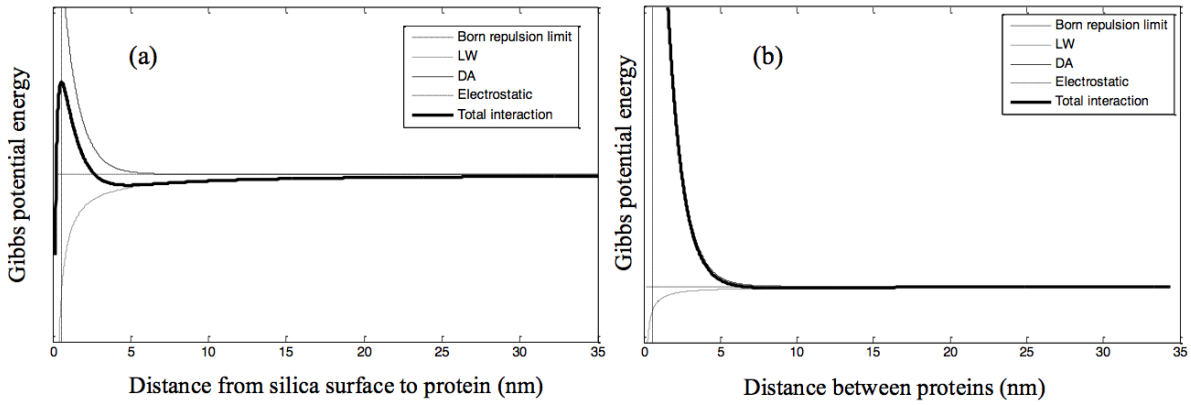

Figure 1: (a) shows an example of the Gibbs distribution of silica - protein in a liquid medium. b) shows an example of the Gibbs distribution of protein - protein in a liquid medium. These are just examples to identify the crucial characteristics of the distributions, so no scale for the Gibbs potential energy was attached.

In the model the silica wafer is treated as a semi-infinite plane occupying the $x-y$ axes at $z = 0$ [18]. The dispersed COE-3 molecules are treated as hard spheres of fixed radius, R [18]. The adsorbed COE-3 layer is described as a fractional semi - infinite plane (FSIP) covering the silica wafer. As more dispersed COE-3 molecules adsorb, the silica wafer becomes saturated and this corresponds to the COE-3 layer being represented as a complete semi - infinite plane.

The adsorption process is modelled by the dispersed COE-3 molecules becoming trapped within the 2^{nd} Gibbs potential minimum, visible in part a) of figure 1, this occurs at $z = a_n$. a_n is a after n adsorbed proteins. The newly adsorbed COE-3 molecule now exerts a repulsive interaction with

incoming COE-3 molecules. This repulsive interaction can be seen in part b) of figure 1. The repulsive COE-3 - COE-3 Gibbs distribution is added to the minimum of the silica - COE-3 Gibbs distribution, signifying adsorption of the protein. This has a shadowing effect on the overall attraction of silica wafer to other dispersed molecules. The additional potential is spread symmetrically across the minimum of the Gibbs distribution in figure 1 a). After a critical number of protein adsorptions N_{max} (FSIP → complete semi-infinite plane) the well is filled. This is when the repulsive FSIP force equals the attractive silica force, signifying saturation. The dispersed molecules no longer feel an attractive force towards the surface. This process is described by

$$G_N(z) = G_{123}(z) + \frac{1}{N_{max}} \begin{cases} \sum_{n=1}^{N} G_{323}(\frac{L_n}{2} + (z - a_{n-1})), & \text{if } z >= a_{n-1} \\ \sum_{n=1}^{N} G_{323}(\frac{L_n}{2} - (z - a_{n-1})), & \text{if } z <= a_{n-1} \end{cases} \tag{16}$$

where N_{max} is the number of COE-3 particles needed to saturate the silica wafer (to fill the potential well). $G_{123}(z)$ is the initial silica - COE-3 interaction. $a_n(L_n)$ is the distribution's minimum after n COE-3 molecules have adsorbed, L_n denotes the width of the well after n adsorptions. It can be seen from the form of the equation 16 that the width of the secondary minimum L_n is defined as the initial Gibbs distribution of the silica - COE-3 interaction at a height above the minimum which is equal to the molecule's root mean square (r.m.s) kinetic energy. For a COE-3 molecule within the FSIP the repulsive forces of the other adsorbed molecules cancel. However, if a molecule desorbs then it will feel a strong FSIP repulsion as this force will no longer cancel in the z direction.

Adsorption, desorption fluxes & the surface adsorbed amount

With an expression for the overall Gibbs potential after N adsorbed molecules, $G_N(z)$, it is now possible to define the flux of incoming COE-3 molecules. After N of N_{max} adsorptions has occurred the flux is

$$F_N = \frac{DC}{\int_{a_N}^{h} e^{\frac{G_N(z)}{k_B T}} dz}. \tag{17}$$

The limits of the integral in the denominator are between the trapping distance, a_N and the maximum height a COE-3 molecule can be above the wafer, h, which is set to $1cm$ [19]. T is the temperature of the solution, D and C are the diffusion coefficient and COE-3 solution concentration respectively. The value of the diffusion coefficient, D was taken to be that of water, $2.4x10^{-9} m^2 s^{-1}$ [20].

In addition to the adsorption flux there is also a desorption flux from the FSIP layer into the medium. This desorption flux has two defining factors. The first is the escape attempt frequency and the second is the escape probability. The attempt frequency is defined as the frequency in which adsorbed molecules collide with the potential barrier between the adsorbed layer and the medium. As L_N is the width of the well, the distance the molecule must travel before colliding with the energy barrier between the FSIP and medium is $2L_N$. Assuming the adsorbed molecules also possess the

r.m.s energy above the minimum of the potential well, the attempt frequency ν_N is

$$\nu_N = \frac{2L_N}{v_{rms}} \tag{18}$$

where $\frac{1}{2}mv_{rms}^2$ is the r.m.s energy. A COE-3 molecule will escape if it possesses sufficient kinetic energy to overcome the potential barrier at the given temperature, T. The total proportion of COE-3 molecules with sufficient kinetic energy can be determined by a Maxwell - Boltzmann distribution, this gives the successful desorption probability, P_N.

Together the adsorption and desorption fluxes govern the total change in the number of adsorbed antibodies in a given time period, Δt, via

$$\Delta N = \frac{F_N A}{m}(1 - \frac{N}{N_{max}})\Delta t - \nu_N P_N N \Delta t \tag{19}$$

with A being the total area of the silica wafer, $(1.2x1.2)cm^2$, the available proportion for adsorption of this area is given by $(1 - \frac{N}{N_{max}})$. N represents the amount of adsorbed COE-3 at the start of the interval, and m is the molecular mass of the protein. Due to computational power limitations, $G_N(z)$ was not computed for each individual molecule. However, it was only computed for certain values of FSIP completion. Equation 19 could then be used to evaluate $N(t)$ iteratively enabling the time dependent surface adsorbed amount could be calculated with

$$\Gamma(t) = N(t)m/A \tag{20}$$

where m is the mass of protein molecules, A is the total area of the wafer and $N(t)$ is the number of adsorbed molecules.

DETERMINING MODEL PARAMETERS

The model required the values of each surface tension component of all three interacting bodies to be known. The total surface tension of a body i, Y_i is known to be made up of the three components γ^{lw}, γ^d and γ^a in the form of equation 2. Components for water and silica could be taken from previous experimental measurements. However, the surface tension components of COE-3 needed to be deciphered.

Determining surface tension components; water, silica & COE-3

The surface tension components of water and silica have been well established for many years, and these components are widely available. The surface tension components for water are known to be $\gamma_2^{lw} = 21.80$ mN/m, $\gamma_2^d = 25.50$ mN/m and $\gamma_2^a = 25.5$ mN/m [14]. The surface tension components for silica are known to be $\gamma_1^{lw} = 39.00$ mN/m, $\gamma_1^d = 4.10$ mN/m and $\gamma_1^a = 0.80$ mN/m [14].

Adsorption conditions and COE-3 - COE-3 interaction map

The surface tension components for COE-3 are not readily available, these needed to be determined. This was done by considering the adsorption conditions that COE-3 must fulfill. These applied restrictions upon the parameter space. Within this restricted parameter space a single collection of components could replicate the experimental data. These values were γ_3^{lw} = 24.35 mN/m, γ_3^d = 31.05 mN/m and γ_3^a = 18.90 mN/m.

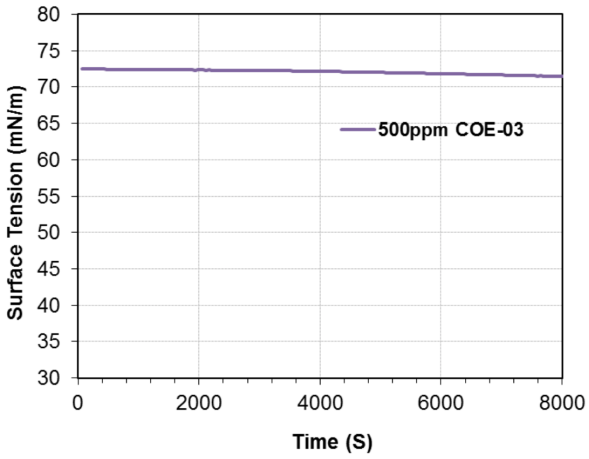

Figure 2: Time dependence of total solution surface tension after 500ppm of COE-3 was added to histidine buffer 25mM at pH 6. Surface tension in mN/m against time in seconds.

Figure 2 shows the change in total surface tension when 500 ppm was added to histidine buffer (25mM, pH 6). It can be seen that the time dependent surface tension of the buffer experiences little change after the addition of COE-3, staying constant at 72.8 mN/m. This suggests COE-3 has a total surface tension similar to water, and this approximation was appropriate to make. Therefore, the total surface tension of COE-3 is $Y_3 = \gamma_3^{lw} + 2\sqrt{\gamma_3^d \gamma_3^a} = 72.8$ mN/m.

To determine the individual components of this total surface tension two adsorption conditions were enforced upon the parameter space. Interactions between molecules can be repulsive, attractive or long range attractive with short range repulsion (abbreviate to type - 2 attraction). The type of interaction that occurs is dependent on the surface tensions of the interacting bodies within the medium. Therefore the first restriction was that COE-3 - COE-3 interactions must be repulsive. If this was not the case than the proteins would accumulate together causing coagulation in the buffer. The LW component is always negative however the DA component can be either negative or positive [10]. The DA component therefore determines the overall interaction. If the DA component is positive this will produce an overall attractive force between the molecules. The factor G_{i2j}^{DA} determines the sign of the DA force. In order to discard the corresponding attractive parameter space the condition that G_{323}^{da} must be negative was enforced

$$G_{323}^{DA} = -2\gamma_{23}^{da} = -4(\sqrt{\gamma_2^d} - \sqrt{\gamma_3^d})(\sqrt{\gamma_2^a} - \gamma_3^a) \begin{cases} > 0, \text{for repulsion \& type 2 attraction} \\ < 0, \text{for attraction.} \end{cases} \tag{21}$$

In addition to $G_{323}^{DA} > 0$ a further condition is needed to ensure type 2 attraction does not occur. This is that $|G_{323}^{LW}| > |G_{323}^{DA}|$, in terms of surface tensions this condition takes the form of

$$|\sqrt{\gamma_3^d - \sqrt{\gamma_2^d}}| > + \frac{(\sqrt{\gamma_2^{lw}} - \sqrt{\gamma_3^{lw}})^2}{2|\sqrt{\gamma_2^a} - \gamma_3^a|}. \tag{22}$$

Another condition was that within the initial Gibbs distribution a minimum must be formed, otherwise initial adsorption would not occur. As previously stated the LW Gibbs potential component is always negative. By also neglecting the electrostatic surface tension contributions a requirement was made. The silica - COE-3 DA interaction must be positive for a minimum to exist within the initial Gibbs distribution. The G_{123}^{DA} factor determines the sign of the silica - COE-3 DA component, this condition took the form of

$$\sqrt{\gamma_3^d} > -\sqrt{\gamma_3^a}\frac{\sqrt{\gamma_2^d} - \gamma_1^d}{\sqrt{\gamma_2^a} - \sqrt{\gamma_1^a}} + \frac{2\sqrt{\gamma_2^a\gamma_2^a} - \sqrt{\gamma_1^a\gamma_2^d} - \sqrt{\gamma_1^d\gamma_2^a}}{\sqrt{\gamma_2^d} - \sqrt{\gamma_1^a}}. \tag{23}$$

Within this restricted parameter space a combination of components could be chosen that possessed sufficiently strong COE-3 - COE-3 repulsion to replicate the experimental data. Figure 3 shows the restricted parameter space and the collection of parameters chosen.

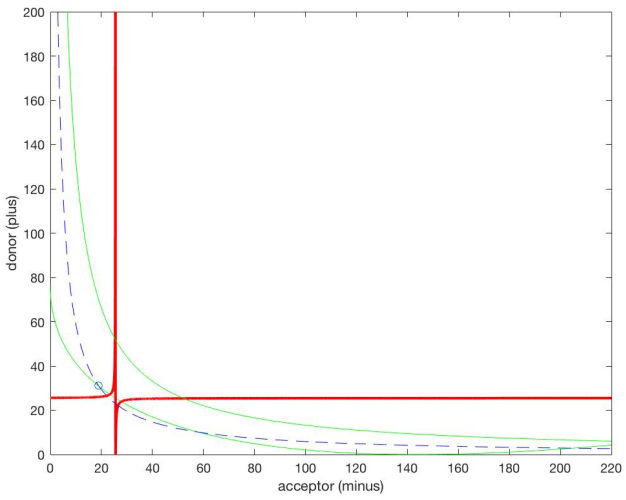

Figure 3: The protein-protein interaction map. The lower green contour represents equation 23, above which a minimum exists in the initial distribution. The higher green contour indicates where γ_3^{lw} is equal to zero. Therefore, between these boundaries lies the region in which protein adsorption onto the silica layer can occur. The contour with γ_3^{lw} = 24.35 mN/m is plotted in the dotted blue. The red contours represent equation 21, above this line in the top left region repulsion exists, whilst repulsion exists below this in the bottom right region. The circle represents the component combination chosen for COE-3; γ_3^{lw} = 24.35 mN/m, γ_3^{d} = 31.05 mN/m and γ_3^{a} = 18.90 mN/m.

Determining surface potentials of COE-3 and silica

The experimental data of the COE-3 charge distribution is shown below.

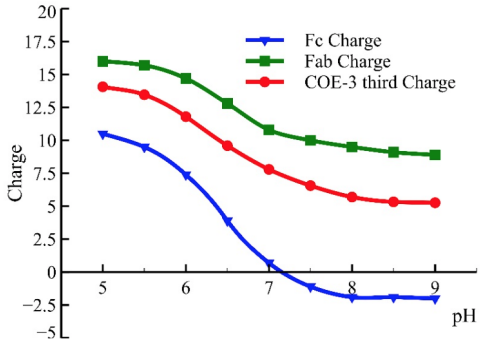

Figure 4: COE-3 surface charge against pH. The charge of the Fc (triangles) and Fab (squares) components of COE-3 are also shown.

The variance of surface potential due to varying buffer environment conditions for silica and COE-3 were found. COE-3 surface potential dependence was found empirically by using the experimental data for surface charge against pH (figure 4) with equation 15. Figure 5 a) shows the result for COE-3.

It can be seen that increases in ionic strength causes the COE-3 surface potential to decrease. An increase in pH also corresponds to a decrease in COE-3 surface potential. Figure 5 b) was produced from equation 13, and shows the surface potential of silica. Silica's surface potential is negative and as pH increases the magnitude of silica's surface potential increases. While an increase in ionic strength decreases the magnitude of silica's surface potential.

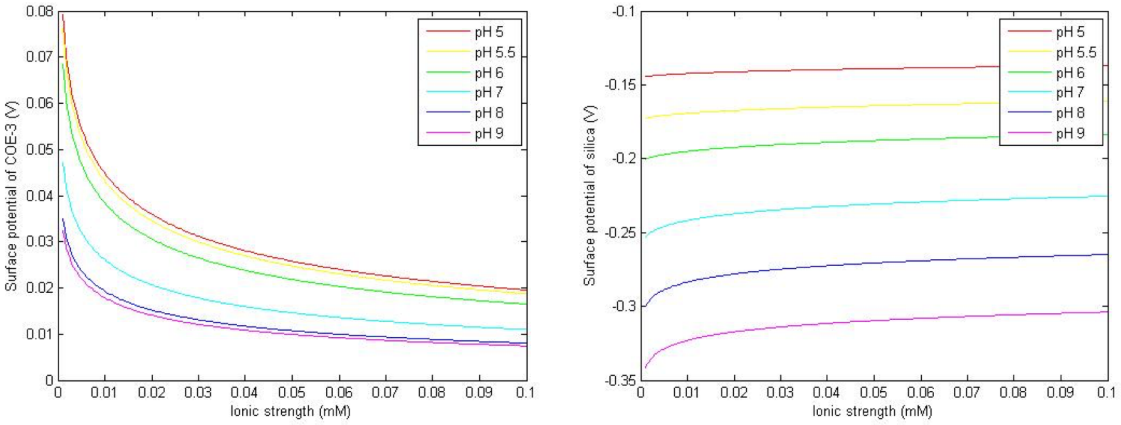

Figure 5: a) COE-3 - COE-3 Surface potentials (Volts), plot of equation 11 over a pH range of 5 to 9 and ionic strengths of 5mM to 100mM. b) COE-3 - silica surface potentials (Volts), plot of equation 13 over pH range of 5 to 9 and ionic strengths of 5mM to 100mM.

Conformation deformations, lateral repulsion & effective COE-3 radii

Although the exact mechanisms remain unclear, it is widely accepted that adsorption and desorption processes cause structural damages [21]. It is also well established that conformational changes occur to antibodies due to different ionic and pH strengths [22]. For simplicity the assumption that COE-3 molecules can be described as hard spheres of fixed radius was made. A weighted average radius of the COE-3 Fab and Fc components was used. The Fab component of COE-3 was taken to be $(85x45x45)$Å^3 and the Fc component of COE-3 was taken to be $(65x75x30)$Å^3 [23]. An average spherical volume consisting of 2 parts Fab and 1 part Fc lead to a hard sphere radius of $R \approx 56$Å. For further simplicity it was also assumed that this radius stays constant within the buffer. However, it is well known that protein conformation drastically changes under the influence of pH and ionic strength [22]. Ionic strength and pH also alter the lateral repulsion experienced between proteins[24]. As a change in ionic strength changes the amount of solution ions binding on to the protein and thus the protein's charge. The protein charge directly relates to the magnitude of lateral repulsion experienced. The model takes account of this in the electrostatic interaction via the α parameter. However, it does not account for the effect of varying lateral repulsion in the adsorbed layer. Therefore, effective radii for COE-3 were used for molecules within the adsorbed layer.

Table 1: pH dependence of FSIP lateral repulsion expressed via an effective radius for COE-3.

pH	Effective radii, Å
5.0	59.5
5.5	58.9
6.0	58.3
7.0	53.5
8.0	49.4
9.0	49.0

Table 2: Ionic strength dependence of FSIP lateral repulsion expressed via an effective radius for COE-3.

Ionic strength (mM)	Effective radii, Å
5.00	56.5
13.26	57.5
25.00	58.3
50.00	61.0
100.00	73.0

These effective radii of COE-3 molecules in the FSIP take into account the pH and ionic strength dependent lateral repulsion within the adsorbed layer [24]. Table 1 and 2 show the corresponding effective radii used for the varying pH and ionic strengths respectively. These were taken from the equilibrated experimental data of 0.2 mg/ml[6] COE-3 concentrations.

RESULTS & DISCUSSION

All simulations were plotted against corresponding experimental measurements taken via Spectroscopic Ellipsometry. The concentration was varied from 0.002 mg/ml to 0.2 mg/ml at fixed pH (pH 6) and ionic strength (25mM). The pH was varied from pH 5 to pH 9 at fixed ionic strength (25mM) for both a high and low COE-3 concentration. The ionic strength was varied from 5mM to 100mM at fixed pH (pH 6) for both a high and low COE-3 concentration. Figures 6, 7 and 8 show COE-3 surface adsorbed amount (Γ) in mg/ml against time in minutes. The adsorption trends have a distinctive rapid initial adsorption followed by a slow plateauing after 1 hour of COE-3 initiation. The slow relaxation period is during which the adsorbed molecules rearrange themselves.

[6]The higher concentration measurements were chosen as these would provide a more accurate account of the dependence of COE-3 equilibrated values to pH and ionic strength.

COE-3 concentration effect

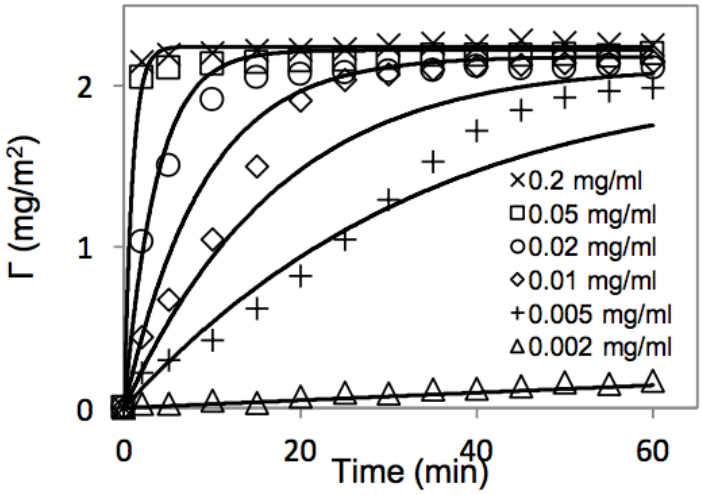

Figure 6: SE measurements (markers) of varying COE-3 concentration, with the y axis representing surface adsorbed amount Γ of COE-3 plotted against time at the Silica/water interface, in a 25mM Histidine buffer, pH 5.5. The bold lines represent the simulation trends of varying COE-3 concentration.

In figure 6 all COE-3 concentrations greater than 0.005 mg/ml show a general convergence towards an adsorption amount of $2mg/m^2$ (pH 5.5, ionic strength 25mM), indicating saturation. As expected the higher the COE-3 concentration corresponds to an increase in adsorbed amount until reaching saturation at $2mg/m^2$. The higher concentrations reached saturation quicker.

In order to provide a good fit to the experimental data an effective concentration had to be used for the lowest experimental COE-3 concentration (0.002 mg/ml, triangles). This effective concentration was an order of magnitude smaller and fitted the experimental trend well. This suggests that the experimental concentration was actually much weaker than 0.002 mg/ml. It also indicates the significant effects of protein adsorption occurring within storage containers. The reason this discrepancy wasn't observed in higher concentrations is due to the storage container losses being a relatively large proportion of the total molecules in weaker concentrations.

Another discrepancy exists between the simulation data and experimental data of the 0.005 mg/ml concentration. The experimental data initial experiences a slower rate of adsorption than the simulation. But, at ≈ 25 minute the experimental adsorption rate surpasses the simulation, ending at a much higher total adsorbed amount than the simulation. One explanation for this discrepancy is due to the hard sphere assumption in the simulation. COE-3 molecules are comprised of two Fabs and one Fc in a Y formation. Baring this in mind, after absorption the molecules can re-orient themselves between head-on, tail-on, side-on and flat-on [25]. This significant rise in experimental adsorption rate could be due to a re-orientation effect from flat-on to a less space consuming orientation (head/tail-on).

Allowing for more COE-3 to adsorb onto this newly freed area. However, the model does not take into account this re-orientating effect. This discrepancy isn't seen in higher concentrations as the initial absorption rate is rapid enough that insufficient time is available for the molecules to re-orientate themselves before saturation.

Overall the simulations presented a good correspondence to the equilibrated (after 60 minutes) experimental data. However, the initial rapid adsorption was not fully captured. This is due to a breakdown of the model at low surface adsorbed amounts. As initially the number of adsorbed COE-3 is small the FSIP approximation (molecules being averaged across the whole surface) does not hold. This corresponds to an overestimation of the repulsive COE-3 - COE-3 interactions. Leading to the initial adsorption to be slower than it is in reality. This deviation between simulation and experimental data is more distinct in the higher COE-3 concentrations.

In figure 6 it can be seen that different concentrations produce different equilibrated adsorbed amounts. On a molecular level the equilibrated amounts represent when the mutual repulsion exerted by the adsorbed COE-3 layer equals the attraction towards the silica. This equality happens at different absorbed amount for different concentrations, leading to the observed concentration effect.

pH effect

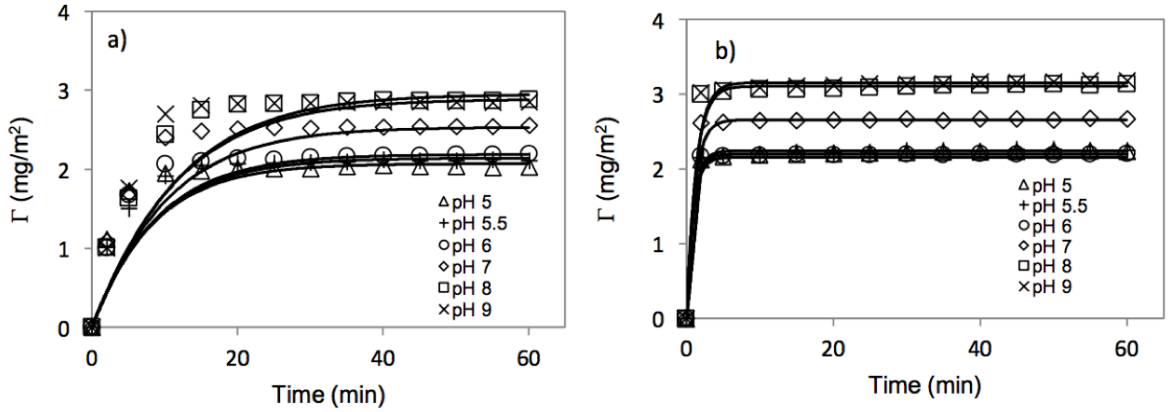

Figure 7: SE measurements (markers) of varying buffer pH, with the y axis representing surface adsorbed amount Γ of COE-3 plotted against time at the Silica/water interface, in a 25mM Histidine buffer, with a) 0.02 mg/ml COE-3 concentration, b) 0.2 mg/ml COE-3 concentration. The bold lines represent the simulation trends of varying pH concentration.

The effects of pH on COE-3 surface adsorption was also investigated for a pH range of 5 to 9. The simulation data was compared to that of Spectroscopic Ellipsometry measurements for two different COE-3 concentrations; one relatively low (0.02mg/ml) and one relatively high (0.2 mg/ml). The total ionic

strength and temperature were keep constant at 25mM and 21°C. A prominent change in absorbed amount due to changing pH was observed. It can be seen from figure 7 that an increase in solution pH results in an increase in the equilibrated adsorbed amount. Where pH 9 shows a saturation level of $3mgm^{-2}$, while pH 5 shows a saturation level of $2mgm^{-2}$.

The order of magnitude difference between COE-3 concentration causes the initial rate of adsorption to be much different. However, the equilibrated values are approximately identical between the two different COE-3 concentrations. This indicates that saturation is achieved in both high and low COE-3 concentrations. A distinct pattern of the final adsorbed amounts is visible in both COE-3 concentrations, being that three trends are clustered above the pH 7 curve and three clustered below the pH 7 curve. The effective radii used were the same for both COE-3 concentrations indicating that this pattern is due to the difference in effective radii between pH values. Which directly relates to the change of lateral repulsion due to pH. This is consistent with previous studies that also suggest that lateral repulsion is the key mechanism in the pH effect [26] [27].

The charge and surface potentials of COE-3 and silica are pH dependent. These dependences are shown in figure 4 and 5. Subsequently, the EL interactions will also be pH dependent. It can be seen from figure 5 that if pH is increased then the COE-3 - COE-3 repulsion will decrease. But, the COE-3 - silica attraction will increase. An overall increase in final adsorbed amounts due to increased pH is expected. This aligns with the experimental data.

The model again underestimates the adsorbed amount of COE-3 over the initial time period. This discrepancy is again due to the unphysical FSIP assumption for low adsorbed COE-3 concentrations as explained before. The inadequate FSIP assumption for small concentrations is further backed up by these results of the pH effect. The higher concentration captures the initial adsorption process, but the lower concentration does not. As the concentration here is higher it means that the dynamic adsorption happens faster making the FSIP assumption valid sooner resulting in a better initial fit, as seen in figure 9 b). In both the low and high concentrations the simulation matches the experimental equilibrated adsorbed amounts, meaning the FSIP assumption becomes valid over a 60 minute time period.

Ionic strength effect

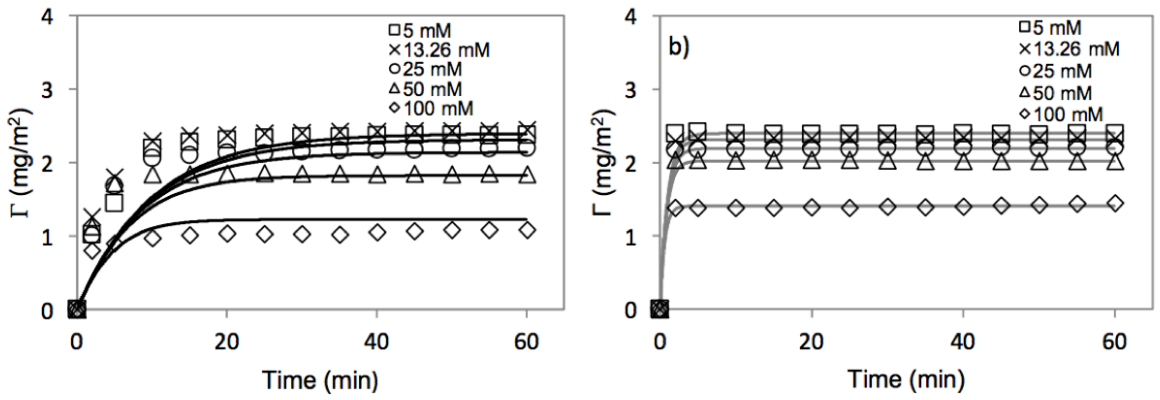

Figure 8: Figure a) shows 0.02mg/ml COE-3 concentration over varying ionic strengths. Figure b) shows 0.2mg/ml COE-3 concentration over varying ionic strengths.

In addition to the pH effect the ionic strength effect on COE-3 surface adsorption was also investigated. This was done for an ionic strength range of 5 to 100 mM. The simulation data was again compared to that of SE measurements for two different COE-3 concentrations; one relatively low (0.02mg/ml) and one relatively high (0.2 mg/ml). The solution pH and temperature was kept constant at pH 6 and 21°C respectively. The initial adsorption dynamics is again underestimated due to the inadequate FSIP assumption for low adsorbed amounts. From figure 8 it can be seen that for both high and low COE-3 concentrations an increase in ionic strength causes a reduction in the adsorbed amount.

The effective radii used to account for lateral repulsion effects in the FSIP was derived from the experimental data of figure 8 b) (0.2 mg/ml concentration). Therefore, the good correlation between the simulation and experimental data seen in figure 8 b) is somewhat artificial. This means figure 8 b) does not provide any insight into the effects of ionic strength. However, the same effective radii were used for the low COE-3 concentration (figure 8 a)) and so this data identifies the key mechanisms of the model that express the ionic strength effects.

Varying ionic strength, and therefore the degree of ion binding alters three variables within the model; electrostatic screening length, the surface potentials and the lateral repulsion within the adsorbed layer.

As ionic strength increases we find that electrostatic screening length decreases which would cause the equilibrated value to decrease. However, beyond the relatively low ionic strength of (>25mM) this effect ceases to change substantially. This is because in equation 12, the Debye screening length,

$\frac{1}{\kappa}$ is inversely proportional to the square root of ionic strength, $\sqrt{I}$. Therefore significant changes of the electrostatic screening length only take effect within a low ionic strength range and so can't fully account for the decrease in final adsorbed amounts observed.

When the effects of ion binding to the COE-3 and the silica surface potentials are also taken into account; the final values for different ionic strengths spread out more. Figure 5 can be used to identifying that the product of surface potentials $\psi_3\psi_3$ (representing COE-3 - COE-3 interactions) decreases less than $\psi_1\psi_3$ (representing silica - COE-3 interactions) over the same increase of ionic strength, 5mM to 100mM. So, a stronger FSIP repulsion relative to silica attraction is present with increased ionic strength, resulting in a decreased adsorption.

Figure 5 also shows that the influence of ionic strength on the surface potentials of silica and COE-3 becomes saturated and plateaus with sufficient increased ionic strength. So this surface potential effect only significantly contributes at low ionic strength. The contribution is too weak to fully account for the decrease in final absorbed amounts observed in Figure 8.

The third variable effected by a greater ionic strength is an increased lateral repulsion amongst the adsorbed layer. This is represented by an increase in the effective radius (occupied area) per an adsorbed COE-3 molecule, resulting in less molecules being able to adhere to the silica.

In order for the simulation to provide a good fit to the experimental results all three of these ionic strength effects (electrostatic screening length, the surface potential variance and the FSIP lateral repulsion) must be included.

CONCLUSION & FURTHER DEVELOPMENTS

The project aimed to produce a DVLO theory based model to help rationalize how changes in concentration, pH and ionic strength influence protein adsorption on a molecular level. The simulations proved to provide good correlations with the experimental data collected. The strong correlation with experimental data indicates that the assumptions made, the DVLO framework used and the COE-3 surface tension components must all hold validity.

Comparisons of the simulations with the experimental data has allowed for an investigation into the driving forces behind important aspects of the adsorption trends. As well as investigating the mechanisms behind the effects of varying environment conditions (ionic strength and pH effects). These aspects were then related to the intrinsic properties of the interacting bodies (COE-3 and silica). It was possible to distinguish the extent of the roles in which lateral repulsion, surface potentials and electrostatic screening played in the effects of varying COE-3 concentration, ionic strength and pH.

It was distinguished that lateral repulsion played the most dominant role at large ionic strengths (50 to 100 mM). However, at lower ionic strengths electrostatic screening had significant decreasing effects to the total adsorbed amounts. In addition, when the ratio of ions to COE-3 molecules was large enough (low COE-3 concentration to high ionic strength), a significant decreasing effect on the total adsorbed amount was present. This was related to the solution ions covering the molecules by a critical amount, altering the surface potentials of COE-3 and the silica surface.

In the pH effect the lateral repulsion was also the major driving force, which was in agreement with previous studies [26] [27]. As pH increases the lateral repulsion decreases leading to an overall increase in total adsorbed amount. The weak pH dependence of COE-3 and silica surface potentials meant that these contributions were magnitudes smaller than that of lateral repulsion.

In low COE-3 concentration solutions the effects of adsorbing molecules within holding containers can be considerable, this was demonstrated by the experimental data for 0.002 mg/ml solution corresponding to a 0.0002 mg/ml simulation. Further highlighting the importance of storage in medical uses of COE-3 and other mAb solutions. The partition of the saturated COE-3 concentrations were shown to be due to the mutual repulsion between the adsorbing and adsorbed COE-3 molecules.

There is potential for further use of the model on different mAb adsorption processes. The model is soon to be tested on other antibodies and its full capabilities will be determined. However, due to the reliance on surface tensions the model can only be used for liquid/solid interface modelling and not gas/solid. Another drawback of the model is the inability to capture the initial adsorption process because of the FSIP assumption being invalid for small adsorbed amounts. Therefore, this important part of the process can not be accurately investigated with the model.

References

[1] Frokjaer S, Otzen DE. Protein drug stability: a formulation challenge. Nature reviews drug discovery. 2005;4(4):298–306.

[2] Behrens SH, Grier DG. The charge of glass and silica surfaces. The Journal of Chemical Physics. 2001;115(14):6716–6721.

[3] Lyklema J. Fundamentals of interface and colloid science: soft colloids. vol. 5. Academic press; 2005.

[4] Derjaguin B. Theory of the stability of strongly charged lyophobic sols and the adhesion of strongly charged particles in solutions of electrolytes. Acta Physicochim USSR. 1941;14:633–662.

[5] Verwey EJW, Overbeek JTG, Overbeek JTG. Theory of the stability of lyophobic colloids. Courier Corporation; 1999.

[6] Israelachvili JN. Intermolecular and surface forces. Academic press; 2011.

[7] Grasso D, Subramaniam K, Butkus M, Strevett K, Bergendahl J. A review of non-DLVO interactions in environmental colloidal systems. Reviews in Environmental Science and Biotechnology. 2002;1(1):17–38.

[8] Couston RG, Skoda MW, Uddin S, van der Walle CF. Adsorption behavior of a human monoclonal antibody at hydrophilic and hydrophobic surfaces. In: Mabs. vol. 5. Taylor & Francis; 2013. p. 126–139.

[9] Main I. Statistical physics, seismogenesis, and seismic hazard. Reviews of Geophysics. 1996;34(4):433–462.

[10] Van Oss CJ. Interfacial forces in aqueous media. CRC press; 2006.

[11] Van Oss C, Ju L, Chaudhury M, Good R. Estimation of the polar parameters of the surface tension of liquids by contact angle measurements on gels. Journal of Colloid and Interface Science. 1989;128(2):313–319.

[12] Salgin S, Salgin U, Bahadir S. Zeta potentials and isoelectric points of biomolecules: the effects of ion types and ionic strengths. Int J Electrochem Sci. 2012;7(12):12404–12414.

[13] Malmberg C, Maryott A. Dielectric Constant of Water from 00 to 1000 C. J Res Nat Bur Stand. 1956;56:369131–8.

[14] Cacace M, Landau E, Ramsden J. The Hofmeister series: salt and solvent effects on interfacial phenomena. Quarterly reviews of biophysics. 1997;30(03):241–277.

[15] Weiner BB, Tscharnuter WW, Fairhurst D. Zeta potential: a new approach. In: Canadian Mineral Analysts Meeting; 1993. p. 1–12.

[16] Ninham BW, Yaminsky V. Ion binding and ion specificity: the Hofmeister effect and Onsager and Lifshitz theories. Langmuir. 1997;13(7):2097–2108.

[17] Giupponi G, Pagonabarraga I. Determination of the zeta potential for highly charged colloidal suspensions. Philosophical Transactions of the Royal Society of London A: Mathematical, Physical and Engineering Sciences. 2011;369(1945):2546–2554.

[18] Cadilhe A, Araújo N, Privman V. Random sequential adsorption: from continuum to lattice and pre-patterned substrates. Journal of Physics: Condensed Matter. 2007;19(6):065124.

[19] Adamczyk Z, Weroński P. Application of the DLVO theory for particle deposition problems. Advances in Colloid and Interface Science. 1999;83(1):137–226.

[20] Holz M, Heil SR, Sacco A. Temperature-dependent self-diffusion coefficients of water and six selected molecular liquids for calibration in accurate 1H NMR PFG measurements. Physical Chemistry Chemical Physics. 2000;2(20):4740–4742.

[21] Perevozchikova T, Nanda H, Nesta DP, Roberts CJ. Protein adsorption, desorption, and aggregation mediated by solid–liquid interfaces. Journal of pharmaceutical sciences. 2015;104(6):1946–1959.

[22] Zhao X, Pan F, Garcia-Gancedo L, Flewitt AJ, Ashley GM, Luo J, et al. Interfacial recognition of human prostate-specific antigen by immobilized monoclonal antibody: effects of solution conditions and surface chemistry. Journal of The Royal Society Interface. 2012;9(75):2457–2467.

[23] Tamada T, Shinmi D, Ikeda M, Yonezawa Y, Kataoka S, Kuroki R, et al. TRAIL-R2 Superoligomerization induced by human monoclonal agonistic antibody KMTR2. Scientific reports. 2015;5.

[24] Zhao X, Pan F, Cowsill B, Lu JR, Garcia-Gancedo L, Flewitt AJ, et al. Interfacial immobilization of monoclonal antibody and detection of human prostate-specific antigen. Langmuir. 2011;27(12):7654–7662.

[25] Xu H, Zhao X, Grant C, Lu JR, Williams DE, Penfold J. Orientation of a monoclonal antibody adsorbed at the solid/solution interface: a combined study using atomic force microscopy and neutron reflectivity. Langmuir. 2006;22(14):6313–6320.

[26] Lu JR, Perumal S, Zhao X, Miano F, Enea V, Heenan RR, et al. Surface-induced unfolding of human lactoferrin. Langmuir. 2005;21(8):3354–3361.

[27] Smith C, Li Z, Holman R, Pan F, Campbell RA, Campana M, et al. Antibody adsorption on the surface of water studied by neutron reflection. In: mAbs. Taylor & Francis; 2017. p. 1–10.